

Article

Microclimate Variation and Estimated Heat Stress of Runners in the 2020 Tokyo Olympic Marathon

Eichi Kosaka ^{1,*}, Akiko Iida ¹ , Jennifer Vanos ², Ariane Middel ³, Makoto Yokohari ¹ and Robert Brown ⁴

¹ Department of Urban Engineering, School of Engineering, University of Tokyo, Tokyo 113-8656, Japan; iida@epd.t.u-tokyo.ac.jp (A.I.); myoko@k.u-tokyo.ac.jp (M.Y.)

² Climate, Atmospheric Science & Physical Oceanography, Scripps Institution of Oceanography, University of California at San Diego, La Jolla, CA 92093, USA; jkvanos@ucsd.edu

³ Department of Geography and Urban Studies, Temple University, Philadelphia, PA 19122, USA; ariane.middel@temple.edu

⁴ Department of Landscape Architecture and Urban Planning, College of Architecture, Texas A&M University, College Station, TX 77843, USA; rbrown@arch.tamu.edu

* Correspondence: ek.at.utf@gmail.com; Tel.: +81-90-6106-0621

Received: 31 March 2018; Accepted: 10 May 2018; Published: 17 May 2018



Abstract: The Tokyo 2020 Olympic Games will be held in July and August. As these are the hottest months in Tokyo, the risk of heat stress to athletes and spectators in outdoor sporting events is a serious concern. This study focuses on the marathon races, which are held outside for a prolonged time, and evaluates the potential heat stress of marathon runners using the COMFA (COMfort Formula) Human Heat Balance (HBB) Model. The study applies a four-step procedure: (a) measure the thermal environment along the marathon course; (b) estimate heat stress on runners by applying COMFA; (c) identify locations where runners may be exposed to extreme heat stress; and (d) discuss measures to mitigate the heat stress on runners. On clear sunny days, the entire course is rated as ‘dangerous’ or ‘extremely dangerous’, and within the latter half of the course, there is a 10-km portion where values continuously exceed the extremely dangerous level. Findings illustrate which stretches have the highest need for mitigation measures, such as starting the race one hour earlier, allowing runners to run in the shade of buildings or making use of urban greenery including expanding the tree canopy.

Keywords: urban microclimate; heat stress; COMFA Human Heat Balance Model; Tokyo 2020 Olympic Games; marathon games

1. Introduction

Heat stress from summer heat is expected to be a significant issue at the 2020 Tokyo Olympics [1]. In recent years, temperatures have risen in the world’s major cities due to both climate change and the urban heat island effect, as caused by the increased longwave radiation from road and building surfaces [2]. These factors have led to an intensification of health hazards posed by heat stress [3,4]. In addition, as Tokyo is located in a temperate zone and has a humid climate, its summers are hot and humid; the Tokyo Olympics are scheduled to be held in July and August in central Tokyo, where the average maximum daily temperature reaches above 30 °C and the average relative humidity reaches over 70%. Consequently, the summer heat and humidity are expected to exert tremendous heat stress on the human body [5–7], and it is estimated to have the poorest conditions among any previous host cities [8,9].

In the outdoor sporting events, heat is expected to impact athletic ability. Of the Olympic events that are held outdoors, marathons require participants to engage in 2–3 h of physical activity in summer

heat; hence, there is a greater chance for negative impacts to the athletes, particularly if less prepared and/or acclimatized. When holding marathons within dense and heterogenous cities, it is necessary to account for the microclimate conditions occurring in urban areas [10–12]. Here, we focus on the conditions on the marathon course and formulate strategies to combat heat stress, such as decreasing solar and longwave radiation by shading with buildings, trees and shrubs [13].

Previous studies investigated the response of marathon runners under serious thermal conditions. Helou et al. [14] studied six marathons in Europe and the United States and found a negative correlation with runners' performance and air temperature, humidity and air pollution. Solar radiation also causes a progressive drop in runners' comfort perception [15], endurance and time to exhaustion [16].

In a study targeting the marathon competition of the Tokyo Olympic Games, Yamazaki et al. [17] assessed the thermal environment on the marathon course using stationary data from the Japan Meteorological Agency. Kashimura et al. [18] measured the thermal environment on the marathon course over three days with a Wet-Bulb Globe Temperature (WBGT) index meter. However, these studies only investigated thermal conditions and did not assess the potential negative effects of high metabolic activities. Because marathon runners continuously perform intense exercise, the high metabolism increases the heat loads on the human body. Therefore, it is necessary to consider these factors to estimate the risks of heat illness for marathon runners.

This study quantifies the thermal comfort and potential heat stress of marathon runners during the 2020 Tokyo Olympic marathon, including human metabolic rate, using the COMFA (COMfort Formula) human heat budget model [19–21], and proposes strategies for improving microclimate conditions on the marathon course to mitigate the heat load and hence the potential heat stress to runners.

2. Methods

2.1. Study Area

This study focuses on the scheduled marathon course for the 2020 Tokyo Olympics (see Figure 1). Runners will start the marathon at the New National Stadium, then pass the Imperial Palace Square, Tokyo Tower, Ginza district and other landmarks in Central Tokyo. They will then reach a turning point at Asakusa, the heart of the old downtown district, where they will double back along the racecourse, finishing the race at the New National Stadium.

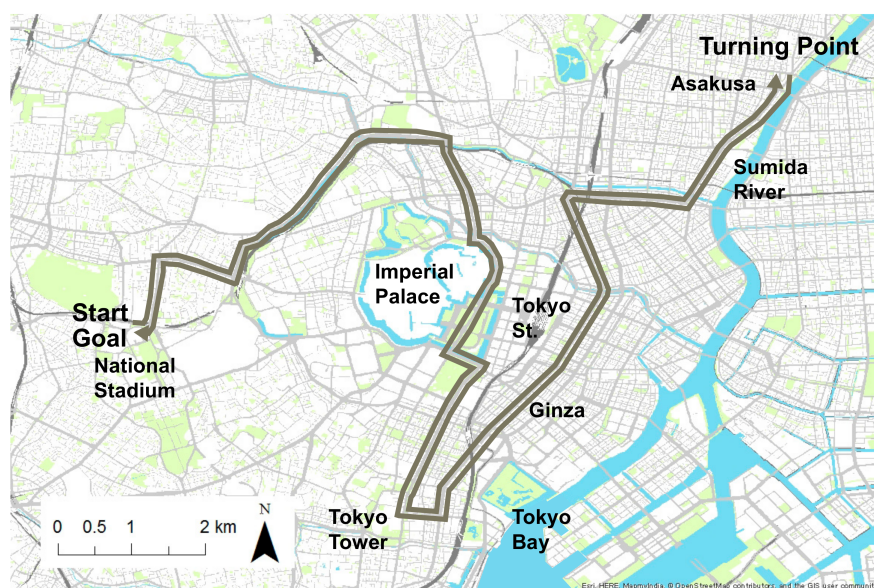


Figure 1. Proposed marathon course for the 2020 Tokyo Olympics.

2.2. Research Methodology

2.2.1. Thermal Environment Measurements along the Marathon Course

Cars and bicycles equipped with weather observation instruments made return trips along the planned marathon course to measure heat conditions along the marathon route. Measurements were conducted in the left-hand traffic lane because runners must run in the left-hand traffic lane in principle, according to the Japan Association of Athletics Federations. This study measured five meteorological elements: air temperature, humidity, solar radiation, road surface temperature and wind speed using the sensors shown in Figure 2. Table 1 provides a list of the weather observation instruments used in this study. POTEKA is a compact weather observation instrument developed by Meisei Electric Co., Ltd. (Ise, Japan) that measures temperature, humidity, solar radiation and wind speed. Surface temperature data were collected by infrared camera, Thermo GEAR G100 (Nippon Avionics Co., Ltd., Shinagawa, Japan). These meteorological elements were linked to ground position using an eTrex 30 GPS (Garmin Ltd., Olathe, USA).

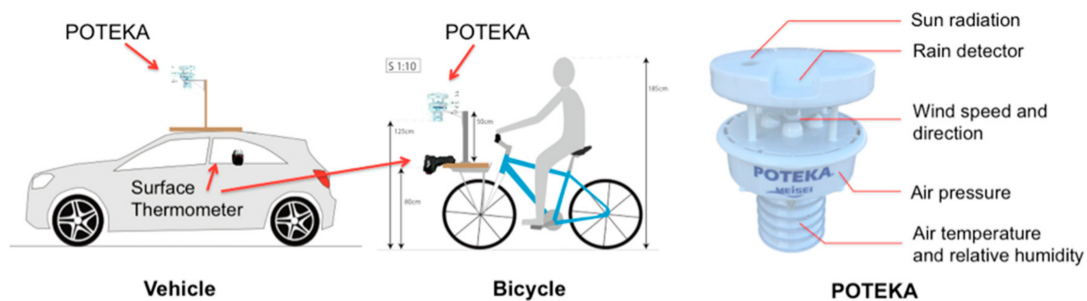


Figure 2. Vehicle and bicycle equipped with weather observation instruments.

Table 1. Summary of mobile meteorological data collection. Meteorological instruments and the accuracy of each use for the mobile data collection. All were measured from an ~1.5-m height apart from the surface temperature.

Instrument	Parameter	Model	Accuracy	Interval
Thermometer	Air Temperature (°C)	POTEKA	±0.3 °C	1 s
Hygrometer	Relative Humidity (%)	POTEKA	±5%	1 s
Pyrometer	Solar Radiation (W/m ²)	POTEKA	±10%	1 s
Surface thermometer	Surface Temperature (°C)	ThermoGEAR G100	±2 °C	3 s
Anemometer	Wind + Activity Speed (m/s)	POTEKA	±1.0 m/s	1 s
GPS	Latitude and Longitude	eTrex30	3 to 6 m	1 s

As shown by d'Ambrosio Alfano et al. (2007), d'Ambrosio Alfano et al. (2013) and Palella et al. (2016), the use of instruments with higher quality provides more accurate and precise results [22–24]; however, among various requirements for the instruments for the given study, the compactness was crucial for the mobile monitoring setups and because the measurements had to be conducted along roads with busy traffic in the 2–3 h morning marathon window. Larger instruments with higher accuracy were not compact enough to be placed on bicycles. The POTEKA, whose accuracy is certified by the Meteorological Agency of Japan, is the best instrument to balance the conflicting requirements of compactness and accuracy.

As shown in Table 2, the measurements were taken for nine days in the summer of 2016, starting at the marathon's scheduled starting time of 7:30 a.m., and for two days starting at 6:30 a.m., one hour earlier than the scheduled start time, for a total of 11 days of measurements. The measurements were taken under a variety of weather conditions: seven clear sunny and four overcast cloudy days. The hottest day was August 9, when the temperature reached a high of 37.9 °C. Furthermore, August 9,

2016 was the hottest day of the year and is the day of the men's marathon during the 2020 Tokyo Olympics. The average high on sunny days was 33.4 °C and on cloudy days was 29.2 °C. According to observational data from the Meteorological Agency, the average temperature, humidity and sunshine hours in 2016 matched the climate norms.

Table 2. List of measurement days, time of measurement and sky conditions.

Date	Time	Sky Condition
Jul 29, 2016	7:30–10:29	sunny
Aug 5, 2016	7:30–10:30	sunny
Aug 6, 2016	7:30–10:31	sunny
Aug 9, 2016	7:30–10:33	sunny
Aug 11, 2016	7:30–9:57	cloudy
Aug 12, 2016	7:30–10:15	cloudy
Aug 13, 2016	7:30–10:16	sunny
Aug 14, 2016	7:30–10:10	cloudy
Aug 23, 2016	6:30–9:20	cloudy
Aug 25, 2016	6:30–9:25	sunny
Aug 26, 2016	7:30–10:25	sunny

Additionally, to ascertain the degree of heat stress risk during a marathon held in the summer in Tokyo, a “worst-case scenario” (representing the potentially warmest environment) and “best-case scenario” (representing the potentially coolest environment) were hypothetically created to supplement the day-by-day data. To create each scenario, the highest and lowest values of each climate factor, excluding solar radiation, were selected from the nine measurement days and synthesized as the data for each scenario. When synthesizing the data, the absolute humidity was calculated with the relative humidity and temperature on the wettest/driest day, and the hypothetical relative humidity was then re-calculated according to the temperature of the warmest/coolest day. Because solar radiation is affected by cloudiness, the highest and lowest values in each section throughout the nine measurement days were used as the data for each scenario.

2.2.2. Estimated Heat Balance of Runners: Application of the COMFA Human Heat Balance Model

Using the measured data, the heat load exerted on the runners from the environment along the marathon route was calculated using the COMFA human heat balance model for each day and scenario. The wind speed was first corrected using the two steps provided in Tokura et al. [25]. First, the stationary wind speed was calculated by subtracting the moving speed of the vehicle or bicycle from the field-measured speed. The moving speed was calculated by positional data of GPS. Second, the wind speed felt by runners (or the relative wind velocity) was calculated by taking the square root of the sum of the squares of the stationary wind speed and runners' average race speed (20 km/h), as in ISO (2007) [26].

To better visualize the distribution of the estimated heat stress along the route, the results for each meteorological factor in the measurement data were divided into 100-m sections; the data recorded in each section for each factor were then averaged and rendered as representative values used in the analysis along the race route.

The COMFA model combines climate factors of temperature, humidity, wind and radiation, with the personal factors of metabolic rate and clothing insulation to estimate thermal comfort and potential heat stress [27–29]. The model defines the energy budget in $W\ m^{-2}$ as follows:

$$B = M + R_{abs} - C - E - L_{emit} \quad (1)$$

where B is the net energy budget, M is metabolic heat production, R_{abs} is the absorbed radiation by a cylindrical human, C is convective heat loss, E is evaporative heat loss (sum of insensible and sensible

heat losses [29]) and L_{emit} is the emitted longwave radiation by a human. All fluxes in Equation (1) are in $W m^{-2}$.

The runners were estimated to have a low clothing insulation (I_{cl}) value of 0.1 clo ($\sim 18.6 s m^{-1}$) based on minimal, thin and low insulation running uniforms and a high amount of exposed skin. We used the sum of the clo values for the individual garments (i.e., $I_{cl} = \sum I_{clu}$) from ISO (2007) based on panties/briefs (0.03 clo) and tank top (0.07 clo).

The COMFA model accounts for the activity of the athlete [20] when calculating thermal comfort and heat stress; however, we are not able to account for inter-individual variability in the current study. An average metabolism of $\sim 700 W m^{-2}$ was determined by allowing for energy to be converted to mechanical work during running, where the net gain from metabolism, M , is $0.8M_{total} + 0.2M_{rest}$ [30], where M_{rest} is 1 MET ($58 W m^{-2}$) and M_{total} is based on running at an average speed of $18 km h^{-1}$ for an elite runner, or 14.5 METs [31]. The influence of an increased relative wind velocity of the runner to promote cooling via decreased resistance to vapor and heat transfer from higher wind is also determined by the COMFA model (see [21,28,32]).

The absorbed radiation was determined from the combined influence of short- and long-wave radiation experienced by a human, based on an effective area of 0.78 for a standing human and average surface (A_{cyl}), using the following equation.

$$R_{abs} = A_{eff} \left(\frac{K_{in(abs)} + K_{up(abs)} + L_{a(abs)} + L_{g(abs)}}{A_{cyl}} \right) \quad (2)$$

where $K_{in(abs)}$ and $K_{up(abs)}$ are the absorbed solar radiation from the sky and ground, respectively, while $L_{a(abs)}$ and $L_{g(abs)}$ are the incoming and outgoing longwave radiation, respectively. The full detailed methods are found in Hardin and Vanos (2017) and Kenny (2008) [33,34]. Below, we outline any changes made from studies [21,28,32] for the given study. The outgoing longwave (L_{out}) radiation was determined from the measured ground temperature and the use of the Stephan–Boltzmann equation. Incoming longwave radiation (L_{in}) was determined based on the summation of infrared energy from the sky or from the buildings. To determine the portion of the sky visible in the upper 180° hemisphere (Sky View Factor (SVF)) in each location, we acquired images via Google Street View and used an SVF calculation methodology by Middel et al. [35–37]. Ninety-degree field of view images were retrieved in four cardinal directions and upwards for all Street View locations that are part of the race course [36]. The images were then segmented into sky versus non-sky pixels using a convolutional neural network [37] and converted into hemispherical fisheye views using equiangular projection. Finally, the SVF value (0–1) was calculated using the modified Steyn method [35].

The absorbed L_{in} ($L_{in(abs)}$) was determined based on the SVF weighting of the longwave emitted from objects in the sky hemisphere (L_o) and longwave from the sky (L_a), as follows:

$$L_a = 213 + 5.5T_a \cdot SVF \quad (3)$$

$$L_o = \epsilon_h \sigma (T_o + 273.15)(1 - SVF) \quad (4)$$

$$L_{in(abs)} = 0.5\epsilon_h(L_o + L_a) \quad (5)$$

Equation (2) is based on Monteith and Unsworth (2008) [38], and the T_o is the temperature of objects in the sky hemisphere, estimated from vertical surface temperature data using an infrared camera (Nippon Avionics, ThermoGear G100, Shinagawa, Japan).

Finally, as per Harlan [39], the calculated human energy budgets were classified into four stages: $>340 W m^{-2}$ are extremely dangerous; $200\text{--}340 W m^{-2}$ are dangerous; $120\text{--}200 W m^{-2}$ are caution; and $<120 W m^{-2}$ are safe.

Convective heat losses were calculated based on a heat flux rate, determined based on the temperature gradient between the skin and air, divided by the resistances (s m^{-1}) to the flow of energy from one surface to the other:

$$C = \rho C_p \left(\frac{T_{sk} - T_a}{r_c + r_a} \right) \quad (6)$$

where ρC_p is the volumetric heat capacity of air, T_{sk} is the skin temperature [21,40], r_c is the clothing resistance (s m^{-1}) and r_a is the boundary air resistance (s m^{-1}) [28].

The evaporative heat loss (E , W m^{-2}) was determined as follows:

$$E = w \left(\rho L_v \left(\frac{q_{sk} - q_a}{r_{cv} + r_{av}} \right) \right) \quad (7)$$

where q_{sk} and q_a are the specific humidity (kg of water vapor per kg of moist air) at T_{sk} and T_a , ρ is the density of air (kg m^{-3}), L_v is the latent heat of vaporization (J g^{-1}), r_{cv} is the clothing vapor resistance (s m^{-1}) and r_{av} is the aerodynamic vapor resistance (s m^{-1}). Vapor resistance calculations can be found in [20,27]. The skin wettedness (w) is calculated as [41]:

$$w = \frac{0.42(M - 58)}{E_{max}} + 0.06 \quad (8)$$

where E_{max} is the maximum amount of evaporative heat loss from the skin (controlled by environmental parameters) (W m^{-2}), calculated as in Equation (7), while holding w at saturation.

2.2.3. Identifying Hot Locations along the Marathon Course

The calculated human energy budget was mapped using ArcGIS 10.2, graphed and visualized to identify locations on the marathon route where runners may be subjected to heat stress. This study primarily examined the results of four cases: August 9, the hottest day of the year in 2016 and the day the men's marathon will be held during the 2020 Tokyo Olympics, the worst-case scenario, the best-case scenario and August 25, a clear, sunny day when measurements were taken one hour early. In addition, the calculated results for each day and each of the two scenarios were compared to estimate the expected degree of heat stress risk during the Tokyo marathons in 2020 and identify locations with high heat loads that lead to poor thermal comfort and heat stress.

The model is not a heat strain model (which refers to the effects on body physiology, such as core temperature or sweat rate leading to heat stroke) that occur due to overall heat loads. Rather, the model focuses on conditions that increase body temperature, including heat loads from physical exertion, ambient temperature and environmental factors (i.e., leading to heat stress) [42]. The COMFA model is a rational model, which is more complex than direct models (such as the Wet-Bulb Globe Temperature) because rational models allow one to change clothing, metabolism, height, weight, etc., internally within the model, which is not possible with direct approaches like the WBGT, humidex or the heat index [43].

2.2.4. Approaches to Mitigate Heat Stress

Based on the locations rated as dangerous for each day and scenario, this study investigated the feasibility of possible methods to mitigate heat stress on the runners, such as by changing the route to increase shade and expanding the tree canopy along the marathon route, greening and the installation of sunshades.

3. Results

3.1. Mean and Standard Deviation of Meteorological Variables

Table 3 shows the average and standard deviation of measurements for all dates and scenarios. When the air temperature exceeds 30°C , the value rises rapidly from the start of measurement, and the

standard deviation is large on many sunny days. In contrast, on cloudy days, the temperature did not reach 30 °C, and the standard deviation was small. Relative humidity was >60% on the majority of days. However, the humidity was lower on August 9 (average of 27%), as the temperature was the highest. The wind speed was nearly constant across all measurement dates. Regarding solar radiation, the maximum value was approximately 1000 W m⁻² on all sunny days, yet the average value and standard deviation varied. On days with clouds, there were greater variations in standard deviation, maximum and average values of solar radiation. A positive association was found between solar radiation and road surface temperature.

Table 3. Mean and standard deviation (SD) of meteorological variables for each day and scenario.

Day or Scenario		T _a (°C)	RH (%)	Wind Speed	Solar Radiation	Road Surface Temperature
				(m s ⁻¹)	(W m ⁻²)	(°C)
29 July	Mean ± SD	29.3 ± 1.26	58.9 ± 4.59	2.0 ± 0.79	427.5 ± 317.76	35.3 ± 5.64
	Range	27.0–32.8	49.1–66.4	0.5–4.4	46.9–1024.1	27.5–49.5
5 August	Mean ± SD	30.8 ± 1.27	58.2 ± 4.65	2.0 ± 0.82	281.1 ± 215.59	36.4 ± 4.43
	Range	28.7–33.9	48.1–65.6	0.5–5.7	51.7–1052.8	29.8–51.4
6 August	Mean ± SD	30.6 ± 1.08	62.2 ± 3.35	1.9 ± 0.69	349.8 ± 238.76	37.7 ± 4.31
	Range	28.2–32.7	55.5–69.8	0.7–4.5	56.1–999.6	30.9–49.0
9 August	Mean ± SD	34.3 ± 1.82	37.0 ± 5.87	2.0 ± 0.88	350.8 ± 249.13	38.6 ± 5.06
	Range	29.6–37.6	29.5–50.3	0.6–8.3	43.2–949.1	27.8–54.8
11 August	Mean ± SD	28.2 ± 0.45	46.2 ± 1.86	1.9 ± 1.19	125.7 ± 95.83	33.4 ± 1.66
	Range	27.1–29.5	42.9–51.2	0.4–10.4	28.3–375.4	30.5–39.4
12 August	Mean ± SD	27.3 ± 0.82	59.0 ± 4.41	1.7 ± 0.87	231.7 ± 83.16	34.2 ± 2.24
	Range	25.9–29.2	49.7–64.6	0.4–10.3	94.4–450.0	29.9–40.6
13 August	Mean ± SD	27.8 ± 0.90	53.5 ± 3.32	1.7 ± 0.82	347.4 ± 193.51	36.1 ± 4.05
	Range	26.3–30.0	48.3–59.9	0.3–6.0	60.3–1066.4	29.5–50.4
14 August	Mean ± SD	26.3 ± 0.85	54.8 ± 3.19	1.7 ± 0.87	253.4 ± 119.17	34.3 ± 3.04
	Range	24.7–28.2	49.1–59.9	0.4–10.7	61.3–727.8	29.0–43.9
23 August	Mean ± SD	27.8 ± 0.96	69.0 ± 3.79	1.9 ± 0.78	101.4 ± 70.31	27.7 ± 1.61
	Range	26.0–29.5	62.2–75.2	0.5–5.0	12.7–399.4	25.1–32.3
25 August	Mean ± SD	29.0 ± 1.07	61.0 ± 4.88	2.0 ± 0.67	203.0 ± 190.22	31.0 ± 4.15
	Range	26.9–31.6	50.4–70.1	0.5–5.4	14.6–824.0	25.4–45.3
26 August	Mean ± SD	30.1 ± 1.09	57.3 ± 3.55	2.0 ± 0.73	311.9 ± 227.17	35.5 ± 5.00
	Range	27.4–32.6	51.0–65.8	0.6–5.1	27.3–1015.9	27.7–50.4
Worst	Reference day	August 9	August 5	August 5	Max of each section	August 9
	Mean ± SD	34.3 ± 1.82	47.4 ± 5.55	2.0 ± 0.82	514.4 ± 276.26	38.6 ± 5.06
	Range	29.6–37.6	38.5–62.1	0.5–5.7	109.8–1066.4	27.8–54.8
Best	Reference day	August 14	August 11	August 13	Min of each section	August 11
	Mean ± SD	26.3 ± 0.85	51.8 ± 3.35	2.0 ± 0.88	97.5 ± 62.94	33.4 ± 1.66
	Range	24.7–28.2	45.6–59.6	0.6–8.3	27.3–341.4	30.5–39.4

Ta: air temperature, RH: relative humidity.

3.2. Maps and Graphs of Human Energy Budget

3.2.1. August 9, 2016

The calculated human energy budgets for August 9 are illustrated in Figures 3 and 4. Given the relatively high air temperatures and extreme relative humidity, conditions considered dangerous occur immediately near the start of the race. One section, which includes a stretch of east-west highway (15.8–17.2 km), runs toward the Sun and had high values of solar radiation and road surface temperatures, so the energy budget exceeded the benchmark for the extremely dangerous level. Values on the homeward route exhibited higher energy budget values as compared to the outward route due to increases in temperature, solar radiation and road surface temperatures as the day progressed. The same stretch of east-west highway on the return path (21.3–22.7 km) also showed an

energy budget that exceeded the extremely dangerous threshold. From 22.8–27.4 km lies a stretch of highway running north-south that was lined with high-rise buildings and is therefore shaded. Thus, the intensity of the solar radiation and road surface temperatures were relatively low compared to other locations, and the energy budget here was almost 100 W m^{-2} lower than for other locations and rated as dangerous. However, from the 27.5-km mark outward, many locations were illuminated by direct solar radiation. Therefore, the road surface temperatures and solar radiation exhibited higher values than in other locations, which resulted in an increase in accumulated temperature and intense longwave radiation, and almost all locations were identified where values exceeded the extremely dangerous level, all the way to the 35.8-km mark. For example, the energy budget in front of the Imperial Palace Square (30.4–31.2 km) ranged from $342.8\text{--}489.5 \text{ Wm}^{-2}$, because there were no tall trees or buildings that could provide shade for runners.

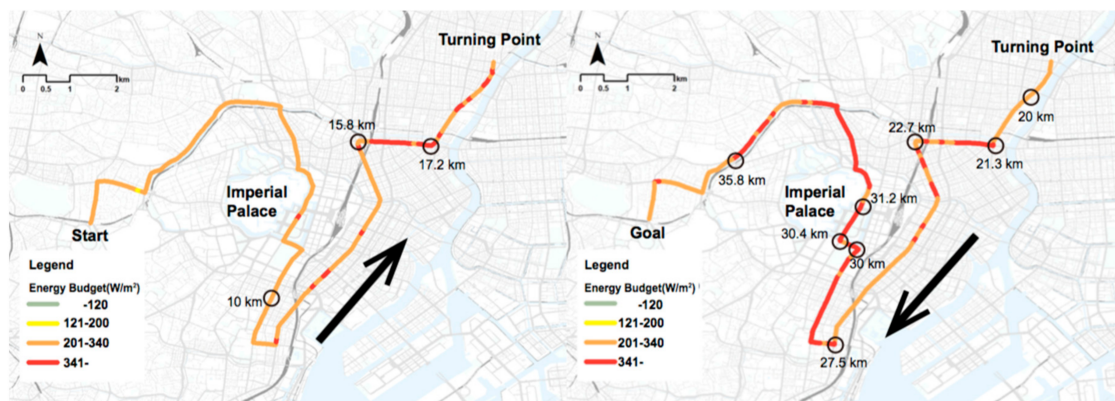


Figure 3. Energy budget for August 9, 2016 mapped on the marathon route (left: outward; right: homeward).

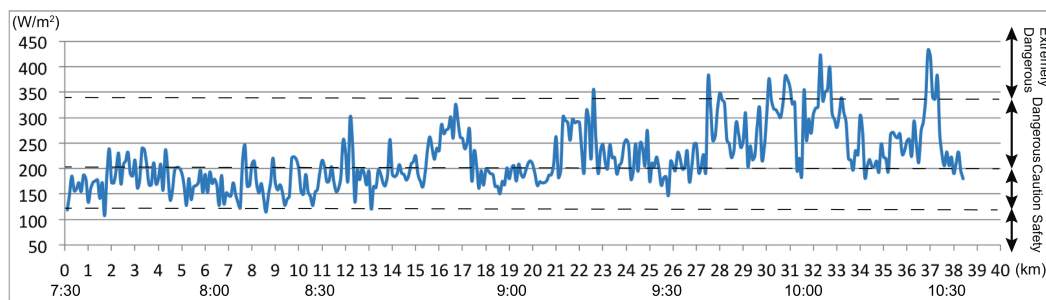


Figure 4. Energy budget for August 9, 2016 graphed as a function of distance.

3.2.2. Worst-Case Scenario

Figures 5 and 6 display the results for the worst-case scenario. In comparison to August 9, the worst-case scenario has higher humidity and lower wind speed. Therefore, the energy budget is higher throughout the entire race, with stretches considered extremely dangerous beginning at the start of the outward transect. The levels of solar radiation in the worst-case scenario show the most intense solar conditions, however, still providing variability due to building and vegetation shading. On August 9, according to data from the Japan Meteorological Agency, at the time of the data collection at the 35.9-km mark, it was overcast, and the Sun was obscured. Therefore, on August 9, the energy budget values after the 35.9-km mark were low. However, the worst-case scenario virtualized clear sunny days, and therefore, the values did not decrease after the 35.9-km mark and exceeded the extremely dangerous threshold from 27.5 to the goal. Based on these results, this section of the route is considered as have a particular need for improvements of the thermal conditions.

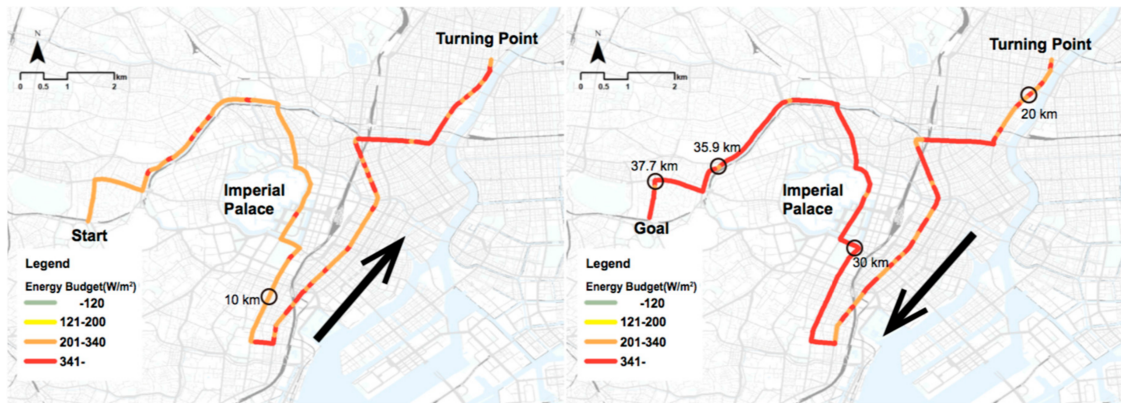


Figure 5. Energy budget for the worst-case scenario mapped on the marathon route (left: outward; right: homeward).

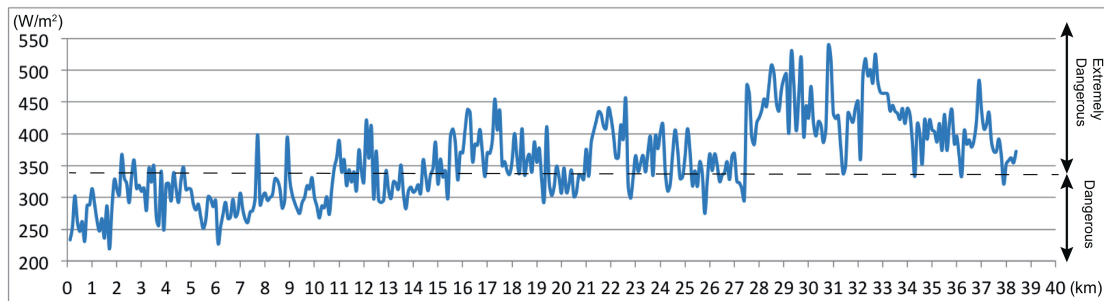


Figure 6. Energy budget for the worst-case scenario graphed as a function of distance.

3.2.3. Best-Case Scenario

Figures 7 and 8 show the results of the best scenario. In this scenario, it is assumed that the route will be constantly overcast, so large changes along the route are not observed, in contrast to August 9 and the worst-case scenario; instead, the energy budget rises gradually with increasing temperature. On the outward route, there is a series of locations evaluated as in the safe range. On the homeward route, the ratings waver between safe and caution, and there are several dangerous spots in the latter half. No spots on the course are evaluated as extremely dangerous.

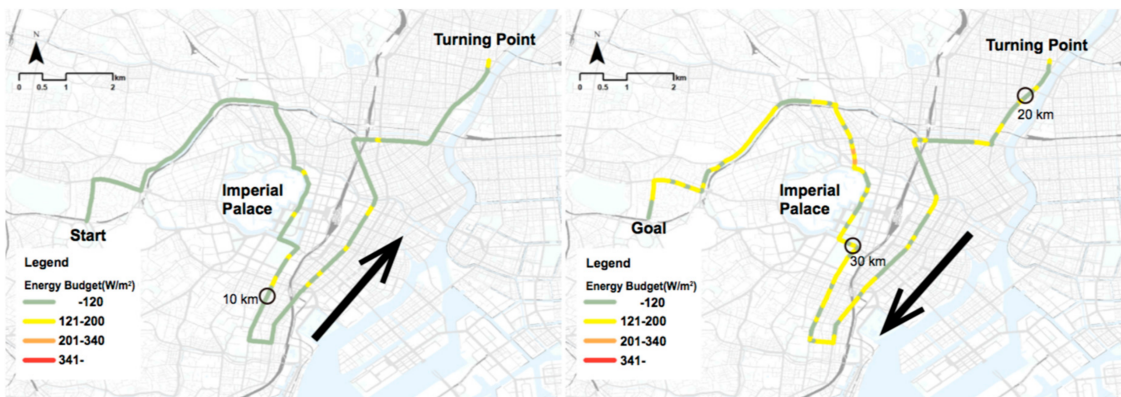


Figure 7. Energy budget for the best-case scenario mapped on the marathon route (left: outward; right: homeward).

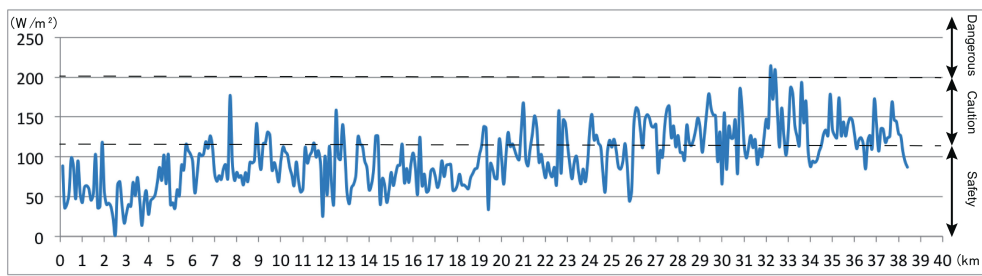


Figure 8. Energy budget for the best-case scenario graphed as a function of distance.

3.2.4. August 25, 2016: Early Start

On August 25, measurements began at 6:30 a.m., an hour earlier than usual. The highest temperature during the measurements was 31.5 °C. It was clear and sunny throughout the measurement period. Therefore, in terms of solar radiation, August 25 was not subject to great weather variability, such as temporary overcast conditions, and each location was considered as subject to the individual maximum solar radiation given the time of day and the presence of vegetation or buildings.

Figures 9 and 10 show the results for August 25. There is a series of dangerous sections on the outward route, but no spots on the outward course are evaluated as extremely dangerous. On the homeward route, just as on August 9 and in the worst-case scenario, high energy budget values are observed from the 27.5-km mark onwards. However, from 28.2–29.9 km and 33.4–36.4 km, the energy budget was lower than those in the surrounding areas. Therefore, as expected, the length of the extremely dangerous area on August 25 is shorter than that of the worst-case scenario. This is largely due to the fact that measurements began an hour earlier than usual, and thus, the solar radiation was at a lower intensity, as well as a significant amount of shade from buildings and trees lining the course remained present.

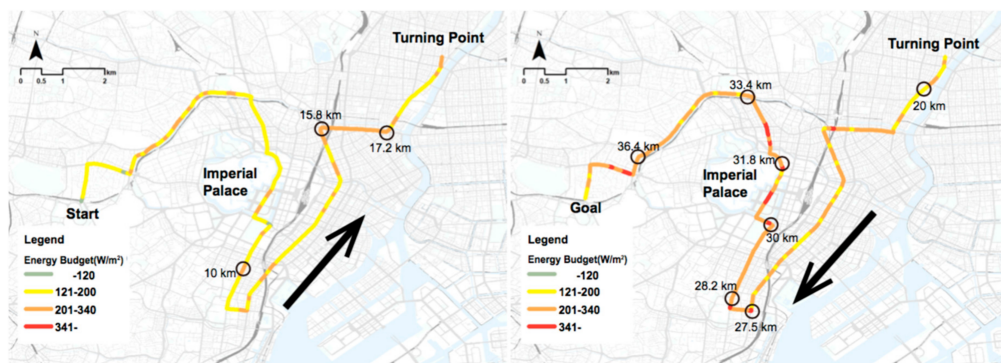


Figure 9. Energy budget for August 25, 2016 mapped on the marathon route (left: outward; right: homeward).

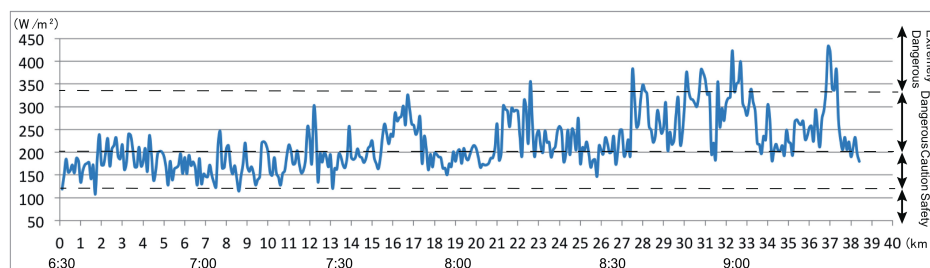


Figure 10. Energy budget for August 25, 2016 graphed as a function of distance.

3.3. Comparison of the Results for Each Case

Table 4 compares the percentage of the overall number of locations rated as safe, caution, dangerous, and extremely dangerous for August 9 and 25 and the worst and best scenarios. For August 9, 29.4% of the total route was rated as extremely dangerous and 70.3% of the total route as dangerous. In the worst-case scenario, 54.9% of the route, almost half the length, was rated as extremely dangerous. In contrast, in the best-case scenario, 70.8% of the route was rated as being in the safe range, with 28.6% of the route rated as dangerous. On August 25, 44.8% was rated as caution, 50.5% as dangerous and 3.9% as extremely dangerous.

Table 4. The percentages of the route rated as safe, caution, dangerous and extremely dangerous for each day and scenario.

	August 9, 2016	Worst Case	BEST CASE	August 25, 2016
Safe	0%	0%	70.8%	0.8%
Caution	0.3%	0%	28.6%	44.8%
Dangerous	70.3%	45.1%	0.6%	50.5%
Extreme Dangerous	29.4%	54.9%	0%	3.9%

Based on these findings, and particularly as demonstrated by the worst-case scenario, sunny, high-temperature and high-humidity conditions produce dangerous conditions throughout the entire route. Consequently, there are some variables that can be modified to improve the thermal environment; nonetheless, heat stress prevention measures are required for the entire course. As with the best-case scenario, even when the skies are overcast and temperatures are not very high, many stretches remain rated as caution or dangerous. Therefore, we believe that a strategy for dealing with heat stress is necessary regardless of the sky conditions, as the temperature and humidity are expected to be at levels considered extreme, and wind speeds are generally low and difficult to alter.

Figure 11 summarizes the heat budget graphs for each measurement date and scenario along the marathon route. Additionally, the course was divided into 25 sections according to the street direction, which is shown on the top bar of Figure 11. Eight sections have a higher energy budget than before and after the sections in the worst-case scenario and on August 9 and 25: (A) 15.8–17.2 km and 21.3–22.7 km, (B) 27.5–27.9 km, (C) 28–29.9 km, (D) 30.4–31.2 km, (E) 31.4–33.3 km, (F) 33.4–34.4 km, (G) 34.5–36.7 km, and (H) 36.8–37.7 km.

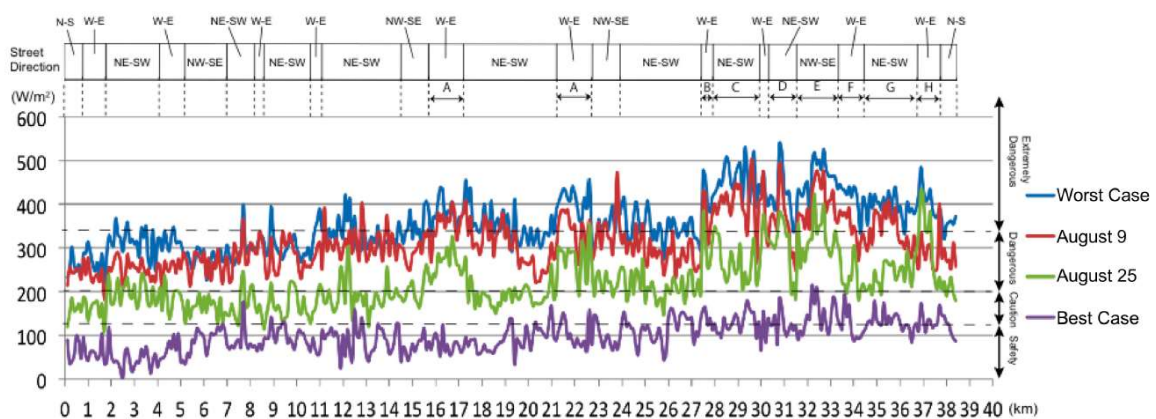


Figure 11. Graphs comparing the heat budget for each day and scenario, including street direction.

3.4. Characteristics of Sections Considered Dangerous

3.4.1. Individual Characteristics of Each Section

Section A (15.7–17.2 km, 21.3–22.7 km)

In these spots, the streets run east-west. Therefore, even though the streets are lined with buildings and trees, they were not able to provide much shade, and the entire street will be in direct sunlight at race time. Therefore, solar radiation and road surface temperatures will be high and the energy budget relatively high in the surroundings.

Section B (27.5–27.9 km)

As is the case with Section A, the streets run east-west. Therefore, even though the streets are lined with buildings and trees, the entire street will be in direct sunlight at race time.

Section C (28–29.9 km)

From 28–28.1 km, there are trees partially blocking the Sun, but the shade does not reach the left lane where the route runs. After that section, there are buildings that partially block the Sun. Based on data from the worst-case scenario and August 9, the Sun will be high in the sky at race time, and the building shadow will not reach the left lane; hence, this area has a high energy budget. However, if the race time is an hour earlier, e.g., as on August 25, the building shade reaches the left lane. Therefore, it has a low energy budget along most of this stretch.

Section D (30.4–31.2 km)

The 30.4–31.1-km section passes through the square in front of the Imperial Palace. There are no trees or buildings present in the surroundings to provide shade, so the solar radiation intensity and road surface temperatures will be high at race time. The energy budget is also high compared to the surroundings, on both the outward and homeward legs. From 31.1–31.2 km, there are trees partially blocking the Sun, but the shade does not reach the left lane. Therefore, it has a high energy budget.

Section E (31.3–33.3 km)

In this section, the Sun is positioned in the southeast, and the streets are almost entirely unshaded at race time, so solar radiation and road surface temperatures will be high.

Section F (33.4–34.4 km)

As is the case with Section A, the streets run east-west. Therefore, even though the streets are lined with buildings and trees, the entire street is in direct sunlight at race time.

Section G (34.5–36.7 km)

In this section, trees are located to partially block the Sun. Data from the worst-case scenario and August 9 and 25 indicate that the trees provide partial shade, so the energy budget will be a little lower than in the surrounding areas. However, where tree growth is poor and tree heights are low, the energy budget will be high.

Section H (36.8–37.7 km)

As is the case with Section A, the streets run east-west. Therefore, even though the streets are lined with buildings and trees, the entire street will be in direct sunlight.

3.4.2. Summary

From the analysis in Section 3.4.1, the energy budget is affected by the locations of buildings and trees that block the Sun relative to the street direction.

Using these data, high energy budget spots on the marathon course were classified into five groups, as shown in Table 5. Group I (A, B, F, H) has shade from trees and buildings, and the road direction is W-E. Group II (C) has shade from trees and buildings, and the road direction is NE-SW. Group III (D, G) has shade only from trees, and the road direction is NE-SW. Group IV (E) has neither trees nor buildings that provide shade, and the road direction is NE-SW. Group V (E) has shade provided by trees and buildings, and the road direction is NW-SE.

In the next section, mitigation approaches are discussed for each group.

Table 5. Classification by the existence of buildings and street trees that block the Sun based on street direction.

	Both Trees and Buildings	Only Trees	Nothing
W-E	A B F H (I)		
NE-SW	C (II)	D G (III)	D (IV)
NW-SE	E (V)		

4. Approaches to Heat Stress Mitigation

The Sun will be facing the flow of traffic; therefore, these sections will be difficult to shade. On the homeward leg, a small amount of shade is present from trees near the road. Therefore, adjusting the tree pruning and expanding the tree canopy so that it projects over the side of the road is a possible measure to consider. It is also hypothesized that installing temporary sunshades to cover the sky above the road could also be effective.

4.1. Group II

The left traffic lane, where the runners will be running, will be unshaded, although there will be some shade in the right traffic lane. Therefore, in this section, the runners should also be allowed to run in the right traffic lane, which will enable them to reduce heat stress.

4.2. Group III

The streets remain unshaded by buildings, but are partially shaded by trees; therefore, expanding the tree canopy will provide more shade. Restricting pruning should expand the canopy and produce more shade on the streets, possibly reducing heat stress on the runners.

4.3. Group IV

As in Group I, there is no shade from buildings or trees. Therefore, it would be desirable to create shade by proactively planting trees along the streets. However, less than three years remain until the Olympics, so more urgent action is necessary, such as placing temporary tree planters and sunshades.

4.4. Group V

The left traffic lane, where the runners will be traveling, will be unshaded, although there will be some shade in the right traffic lane. Therefore, in this section, at first, the runners should also be allowed to run in the right traffic lane. Second, adjusting tree pruning and expanding the tree canopy and the installation of temporary sunshades to cover the sky above the road would be an improvement.

5. Conclusions

This study estimated the potential heat load that runners would be exposed to during the planned course of the marathon in the 2020 Tokyo Olympics. These findings were used to propose possible methods for reducing that stress. The primary findings are as follows.

1. On clear sunny days (the worst-case scenario), many stretches along the course were rated as dangerous or extremely dangerous. In particular, the stretch from 27.5 km–37.7 km is dominated by race segments in direct sunlight and had near-continuous sections that significantly exceeded the extremely dangerous standard. This section is in particular need of measures to improve heat stress conditions.
2. Under cloudy weather (the best-case scenario), from the start of the race, there were stretches that were rated as at the safe level. However, in the second half of the race, there were stretches rated as caution. Therefore, even under conditions that are the coolest for the given time of year, it is necessary to take measures against heat stress.
3. Starting the race one hour earlier would decrease race temperatures and increase the number of shaded sections on the return route. These results suggest that starting the race one hour earlier would be an effective measure against heat stress by shortening the continuous stretches rated as extremely dangerous, as demonstrated by comparing data gathered using the race's scheduled start time.
4. Based on the classified sections along the course, we propose: (1) allowing runners to run in the shade of buildings, (2) making use of urban greenery, such as expanding the tree canopy, and (3) placing temporary tree planters and sunshades as three effective strategies for reducing the heat stress from the Sun and longwave radiation.

To summarize, the current marathon course is considered extremely high-risk for heat stress, particularly on the homeward course, with its high percentage of stretches in direct sunlight. In addition, the risk of heat stress is present even during overcast weather. Therefore, there is a need for measures to reduce the overall heat load caused by the sun and longwave radiation, tailored to the characteristics of individual segments; measures to reduce the effective temperature on runners throughout the entire course and an earlier race start time than currently scheduled would be effective at reducing heat stress.

The following two points should also be considered as future research topics. First, this study identified connected stretches evaluated as extremely dangerous for the runners during the planned homeward course for the marathon competition in the Tokyo Olympics. However, whether these stretches could potentially inflict a serious impact on the runners, and cause them to quit the race, cannot be evaluated based solely on the results of this study. Although preceding literature refers to core body temperature, which is correlated with the risks of heat stress, gradually increasing in the dangerous thermal environment while skin temperature increases rapidly [44], the effect of heat accumulation on core body temperature is still not well discussed. Further research that investigates the effect of heat accumulation on human health is therefore suggested. Second, measures to reduce heat stress were discussed in Section 4, but their degree of effectiveness on a person moving at a certain speed and not stopping in any one place for a long period of time, such as a runner, remains unknown; again, further research is necessary.

Author Contributions: The authors declare that each have contributed equally to the production of this document, whereby: (i) E.K., A.I. and M.Y. performed the measurement and analyzed the data; (ii) J.V. and R.B. contributed to the calculation of the COMFA energy budget; and (iii) A.M. calculated the sky view factor. All authors aided in the writing and reviewing of the manuscript.

Funding: This research received no external funding.

Acknowledgments: Thermal environment measurements were conducted in collaboration with Shimizu Corporation. The weather observation instrument "POTEKA" was provided by Meisei Electric Corporation.

Conflicts of Interest: The authors declare no conflict of interest.

References

1. Tokyo Metropolitan Government Environment Bureau. Available online: <https://www.kankyo.metro.tokyo.jp/climate/other/countermeasure/suishinkaigi.html> (accessed on 16 June 2017). (In Japanese)
2. Golden, J.S. The built environment induced urban heat island effect in rapidly urbanizing arid regions—A sustainable urban engineering complexity. *Environ. Sci.* **2003**, *1*, 321–349. [[CrossRef](#)]
3. Tan, J.; Zheng, Y.; Tang, X.; Guo, C.; Li, L.; Song, G.; Zhen, X.; Yuan, D.; Kalkstein, A.; Li, F.; et al. The urban heat island and its impact on heat waves and human health in Shanghai. *Int. J. Biometeorol.* **2010**, *54*, 75–84. [[CrossRef](#)] [[PubMed](#)]
4. Patz, J.A.; Campbell-Lendrum, D.; Holloway, T.; Foley, J.A. Impact of regional climate change on human health. *Nature* **2005**, *438*, 310–317. [[CrossRef](#)] [[PubMed](#)]
5. Nakai, S.; Itoh, T.; Morimoto, T. Deaths from heat-stroke in Japan: 1968–1994. *Int. J. Biometeorol.* **1999**, *43*, 124–127. [[CrossRef](#)] [[PubMed](#)]
6. Wetterhall, S.F.; Coulombier, D.M.; Herndon, J.M.; Zaza, S.; Cantwell, J.D. Medical care delivery at the 1996 Olympic Games. *J. Am. Med. Assoc.* **1998**, *279*, 1463–1468. [[CrossRef](#)]
7. Zhang, J.J.; Wang, L.D.; Chen, Z.; Ma, J.; Dai, J.P. Medical care delivery at the Beijing 2008 Olympic Games. *World J. Emerg. Med.* **2011**, *2*, 267–271. [[CrossRef](#)] [[PubMed](#)]
8. Kakamu, T.; Wada, K.; Smith, D.R.; Endo, S.; Fukushima, T. Preventing heat illness in the anticipated hot climate of the Tokyo 2020 Summer Olympic Games. *Environ. Health Prev. Med.* **2017**, *22*, 68. [[CrossRef](#)] [[PubMed](#)]
9. Smith, K.R.; Woodward, A.; Lemke, B.; Otto, M.; Chang, C.J.; Mance, A.A.; Balmes, J.; Kjellstrom, T. The last Summer Olympics? Climate change, health, and work outdoors. *Lancet* **2016**, *388*, 642–644. [[CrossRef](#)]
10. Huang, L.; Li, J.; Zhao, D.; Zhu, J. A fieldwork study on the diurnal changes of urban microclimate in four types of ground cover and urban heat island of Nanjing, China. *Build. Environ.* **2008**, *43*, 7–17. [[CrossRef](#)]
11. Miyazaki, H.; Moriyama, M.; Yoshida, A. Field study on green canopy as urban cool-spot. *Nat. Hum. Act.* **1996**, *1*, 51–56.
12. Middel, A.; Häb, K.; Brazel, A.J.; Martin, C.; Guhathakurta, S. Impact of urban form and design on microclimate in Phoenix, AZ. *Landsc. Urban Plan.* **2014**, *122*, 16–28. [[CrossRef](#)]
13. Middel, A.; Selover, N.; Hagen, B.; Chhetri, N. Impact of shade on outdoor thermal comfort—A seasonal field study in Tempe, Arizona. *Int. J. Biometeorol.* **2016**, *60*, 1849–1861. [[CrossRef](#)] [[PubMed](#)]
14. Helou, N.E.; Tafflet, M.; Berthelot, G.; Tolaini, J.; Marc, A.; Guillaume, M.; Hausswirth, C.; Toussaint, J.F. Impact of environmental parameters on marathon running performance. *PLoS ONE* **2012**, *7*, e37407. [[CrossRef](#)] [[PubMed](#)]
15. Hodder, S.G.; Parsons, K. The effects of solar radiation on thermal comfort. *Int. J. Biometeorol.* **2007**, *51*, 233–250. [[CrossRef](#)] [[PubMed](#)]
16. Otani, H.; Kaya, M.; Tamaki, A.; Watson, P.; Maughan, R.J. Effects of solar radiation on endurance exercise capacity in a hot environment. *Eur. J. Appl. Physiol.* **2016**, *116*, 769–779. [[CrossRef](#)] [[PubMed](#)]
17. Yamasaki, Y.; Tsunematsu, N.; Yokohama, H.; Umeki, K.; Honjo, T. Prediction of Thermal Environment in Olympic Marathon Course by Thermal Comfort Map. *Environ. Inf. Sci.* **2016**, *30*, 43–48. (In Japanese)
18. Kashimura, O.; Minami, K.; Hoshi, A. Prediction of WBGT for the Tokyo 2020 Olympic Marathon. *Jpn. J. Biometeorol.* **2016**, *53*, 139–144.
19. Brown, R.D.; Gillespie, T.J. *Microclimatic Landscape Design: Creating Thermal Comfort and Energy Efficiency*; Wiley: Hoboken, NJ, USA, 1995; pp. 1–208.
20. Vanos, J.K.; Warland, J.S.; Gillespie, T.J.; Kenny, N.A. Improved predictive ability of climate–human–behaviour interactions with modifications to the COMFA outdoor energy budget model. *Int. J. Biometeorol.* **2012**, *56*, 1065–1074. [[CrossRef](#)] [[PubMed](#)]
21. Brown, R.D.; Gillespie, T.J. Estimating outdoor thermal comfort using a cylindrical radiation thermometer and an energy budget model. *Int. J. Biometeorol.* **1986**, *30*, 43–52. [[CrossRef](#)] [[PubMed](#)]
22. d’Ambrosio Alfano, F.R.; Palella, B.I.; Riccio, G. The role of Measurement Accuracy on the Heat Stress Assessment according to ISO 7933: 2004. *WIT Trans. Biomed. Health* **2007**, *11*, 115–124.
23. d’Ambrosio Alfano, F.R.; Dell’Isola, M.; Palella, B.I.; Riccio, G.; Russi, A. On the measurement of the mean radiant temperature and its influence on the indoor thermal environment assessment. *Build. Environ.* **2013**, *63*, 79–88. [[CrossRef](#)]

24. Palella, B.I.; Quaranta, F.; Riccio, G. On the management and prevention of heat stress for crews onboard ships. *Ocean Eng.* **2016**, *112*, 277–286. [[CrossRef](#)]
25. Tokura, H.; Nabeshima, M.; Nisioka, M.; Nakao, M. Mobile observation method for spatial variation of direction and velocity of wind on grand level. *Proc. Res. Meet. Arch. Inst. Jpn. Kinki Branch (Environment)* **2007**, *47*, 289–292. (In Japanese)
26. *ISO 9920: Ergonomics of the Thermal Environment: Estimation of Thermal Insulation and Water Vapour Resistance of a Clothing Ensemble*; ISO: Geneva, Switzerland, 2007.
27. Kenny, N.A.; Warland, J.S.; Brown, R.D.; Gillespie, T.G. Part A: Assessing the performance of the COMFA outdoor thermal comfort model on subjects performing physical activity. *Int. J. Biometeorol.* **2009**, *53*, 415–428. [[CrossRef](#)] [[PubMed](#)]
28. Kenny, N.A.; Warland, J.S.; Brown, R.D.; Gillespie, T.G. Part B: Revisions to the COMFA outdoor thermal comfort model for application to subjects performing physical activity. *Int. J. Biometeorol.* **2009**, *53*, 429–441. [[CrossRef](#)] [[PubMed](#)]
29. Vanos, J.K.; Warland, J.S.; Gillespie, T.J.; Slater, G.A.; Brown, R.D.; Kenny, N.A. Human energy budget modeling in urban parks in Toronto, ON and applications to emergency heat stress preparedness. *J. Appl. Meteorol. Climatol.* **2012**, *51*, 1639–1653. [[CrossRef](#)]
30. De Freitas, C.R.; Dawson, N.J.; Young, A.A.; Mackey, W.J. Microclimate and heat stress of runners in mass participation events. *J. Clim. Appl. Meteorol.* **1985**, *24*, 184–191. [[CrossRef](#)]
31. Ainsworth, B.E.; Haskell, W.L.; Herrmann, S.D.; Meckes, N.; Bassett, D.R., Jr.; Tudor-Locke, C.; Greer, J.L.; Vezina, J.; Whitt-Glover, M.C.; Leon, A.S. Compendium of Physical Activities: A second update of codes and MET values. *Med. Sci. Sports Exerc.* **2011**, *43*, 1575–1581. [[CrossRef](#)] [[PubMed](#)]
32. Vanos, J.K.; Herdt, A.J.; Lochbaum, M.R. Effects of physical activity and shade on the heat balance and thermal perceptions of children in a playground microclimate. *Build. Environ.* **2017**, *126*, 119–131. [[CrossRef](#)]
33. Hardin, A.W.; Vanos, J.K. The influence of surface type on the absorbed radiation by a human under hot, dry conditions. *Int. J. Biometeorol.* **2018**, *62*, 43–56. [[CrossRef](#)] [[PubMed](#)]
34. Kenny, N.A.; Warland, J.S.; Brown, R.D.; Gillespie, T.G. Estimating the radiation absorbed by a human. *Int. J. Biometeorol.* **2008**, *52*, 491–503. [[CrossRef](#)] [[PubMed](#)]
35. Middel, A.; Lukasczyk, J.; Maciejewski, R. Sky View Factors from synthetic fisheye photos for thermal comfort routing—A case study in phoenix, Arizona. *Urban Plan* **2017**, *2*, 19–31. [[CrossRef](#)]
36. Middel, A.; Lukasczyk, J.; Maciejewski, R.; Demuzere, M.; Roth, M. Sky view factor footprints for urban climate modeling. *Urban Clim.* **2018**, under review.
37. Lukasczyk, J.; Middel, A.; Zakrzewski, S.; Arnold, M.; Maciejewski, R. Urban Form and Composition of Street Canyons: A Human-Centric Big Data and Deep Learning Approach. *Landsc. Urban Plan.* **2018**, under review.
38. Monteith, J.L.; Unsworth, M.H. *Principles of Environmental Physics*, 3rd ed.; Academic Press: New York, NY, USA, 2008; pp. 1–418.
39. Harlan, S.L.; Brazel, A.J.; Prashad, L.; Stefanov, W.L.; Larsen, L. Neighborhood microclimates and vulnerability to heat stress. *Soc. Sci. Med.* **2006**, *63*, 2847–2863. [[CrossRef](#)] [[PubMed](#)]
40. Vanos, J.K.; Warland, J.S.; Gillespie, T.J.; Kenny, N.A. Thermal comfort modelling of body temperature and psychological variations of a human exercising in an outdoor environment. *Int. J. Biometeorol.* **2012**, *56*, 21–32. [[CrossRef](#)] [[PubMed](#)]
41. Havenith, G.; Holmer, I.; Parsons, K.C. Personal factors in thermal comfort assessment: Clothing properties and metabolic heat production. *Energy Build.* **2002**, *34*, 581–591. [[CrossRef](#)]
42. Vanos, J.K.; Warland, J.S.; Gillespie, T.J.; Kenny, N.A. Review of the physiology of human thermal comfort while exercising in urban landscapes and implications for bioclimatic design. *Int. J. Biometeorol.* **2010**, *54*, 319–334. [[CrossRef](#)] [[PubMed](#)]
43. Hosokawa, Y.; Grundstein, A.J.; Vanos, J.K.; Cooper, E.R. Environmental Condition and Monitoring. In *Sport and Physical Activity in the Heat*; Casa, D.J., Ed.; Springer: Cham, Switzerland, 2018; pp. 147–162.
44. Höppe, P. Different aspects of assessing indoor and outdoor thermal comfort. *Energy Build.* **2002**, *34*, 661–665. [[CrossRef](#)]

